Journal of Applied Fluid Mechanics, Vol. 9, No. 3, pp. 1057-1071, 2016.
Available online at www.jafmonline.net, ISSN 1735-3572, EISSN 1735-3645.
DOI: 10.18869/acadpub.jafm.68.228.24144

Numerical Investigation of the Water Droplet Transport in a PEM Fuel Cell with Serpentine Flow Channel

B. Mondal[1, 2] and D. Chatterjee[1†]

[1] *Simulation & Modeling Laboratory CSIR-Central Mechanical Engineering Research Institute, Durgapur-713209, India*
[2] *Presently on Deputation at the Department of Mechanical Engineering Texas A & M University, TX 77843-3123, USA*

†*Corresponding Author Email: rsdchat@yahoo.co.in*

(Received October 9, 2014; accepted April 29, 2015)

ABSTRACT

The serpentine flow channel can be considered as one of the most common and practical channel layouts for a polymer electrolyte membrane fuel cell (PEMFC) since it ensures an effective and efficient removal of water produced in a cell with acceptable parasitic load. Water management is one of the key issues to improve the cell performance since at low operating temperatures in PEMFC, water vapor condensation starts easily and accumulates the liquid water droplet within the flow channels, thus affecting the chemical reactions and reducing the fuel cell performance. In this article, a comprehensive three dimensional numerical simulation is carried out to understand the water droplet mobility in a serpentine gas flow channel for a wide range of surface properties, inlet air velocities, droplet positions (center or off-center, bottom or top) and droplet sizes by deploying a finite volume based methodology. The liquid-gas interface is tracked following the volume-of-fluid (VOF) method. The droplet transport is found to be greatly influenced by the surface wettability properties, inlet velocities, number of droplets emerged and initial droplet positions. Super hydrophobic surface property is not always preferable for designing the gas flow channels. It depends upon the inlet velocity conditions, droplet positions, number of droplets and surface properties.

Keywords: 3-Dimensional; Serpentine Flow Channel; PEM Fuel Cell; VOF Method; Droplet Transport; Wettability Properties.

NOMENCLATURE

$\vec{F}$	external force term (n)	$\vec{v}$	velocity vector (m/sec)
$\vec{g}$	gravitational force(m/sec^2)		
p	pressure term (n/m^2)	ρ	density (kg/m^3)
t	time (sec)	σ	surface tension coefficient (n/m)
Superscript		μ	dynamic viscosity (kg/m-sec)
T	transpose		

1. INTRODUCTION

Polymer electrolyte membrane fuel cells (PEMFC) are a clean power source and have been emerged as one of the most promising advanced energy technologies particularly as alternative sources in automotive and backup power applications (Martemianov 2009). The PEMFC is efficient, environmental friendly, quiet and simple in design and operation. The performance of PEMFC is significantly influenced by the flow distributions in the flow channels and gas diffusion layer (GDL) since water flooding and concentration distribution are one of the key issues governed by the configurations of flow channel layouts. To avail the high proton conductivity, the water generated on the cathode side is used to hydrate the membrane but excessive water may cause flooding in the reaction zone, GDL and flow channels which reduces the oxygen supply in the reaction zone. At the low operating temperatures in PEMFC, water vapor condensation starts easily and accumulates the liquid water droplet within the flow channels, thus affecting the chemical reactions and thereby reducing the cell performance. The droplet mobility strongly depends on the surface wettability

properties and gas flow conditions. Therefore, a comprehensive study on the droplet mobility for a wide range of surface wettability properties of a serpentine flow channel PEMFC needs to be carried out to understand the mechanism in a greater detail. It should be recognized that the serpentine flow channel layout is a widely chosen design for PEMFC since it ensures effective removal of water from the cell without causing a significant pressure drop (Park 2007).

The study on the water management in PEMFC has emerged in recent years, involving both experimental as well as numerical interventions. Qi (2002) proposed an improvement to the water management using a micro-porous sub-layer for PEMFC. Nguyen (2003) developed the sequential exhausting cell method to overcome the problem of flooding due to deficient flow of gas. A water-flux model for vapor and liquid phases through a gas flow channel was developed by Yi (2004). They introduced a novel intra-cell water-exchange method that is capable of removing and supplying water within a cell depending on the local demand. Jiao (2006a, 2006b) investigated the liquid water transport in straight channels as well as serpentine channels of PEM fuel cell stacks using the volume-of-fluid (VOF) method. Experimental investigations were also carried out on liquid water removal from the gas diffusion layer by reactant flow in a PEM fuel cell (Jiao 2010). Wang (2012) performed an experimental study on super hydrophobic flow channels and showed that super hydrophobic channels enhanced the water removal rate due to lower resistance to the two phase water-air flow in the channel and it improved the PEMFC performance. A hydrophilic small size needle was inserted in the middle of a conventional channel to improve the water removal and transport in the channel by Qin (2013). This study mainly focused on the improvement of water management of PEMFC.

The effects of surface polytetrafluoroethene (PTFE) coverage, channel geometry and air flow rate on the liquid droplet deformation on GDL surface were experimentally investigated (Kumbur 2006). Cho (2012) studied the dynamics of water droplet in a straight flow channel through theoretical and numerical techniques. Theodorakakos (2006) performed experimental studies to estimate the relationship between gas flow rates, the degree of droplet deformation and the force balance acting on the droplet. Lu (2010) studied water management in PEMFC experimentally. Two-phase flow in PEMFC cathode parallel channel was investigated over a wide range of superficial air and water velocities in a specially designed ex situ experimental setup. Golpaygan (2011) studied numerically the dynamics of water droplet in PEMFC by using the VOF method and reported effects of the Reynolds number and Capillary number on water droplet dynamics. Mondal (2011) simulated the water droplet movement in a straight flow channel of PEMFC with hydrophilic surfaces and reported that the droplet transport depends on the inlet air velocity, surface wettability properties etc. The pore location and the wettability of the sidewall play important roles on the water droplet movement in a flow channel of a PEMFC (Zhu 2011). Bunmark (2010) developed an innovative flow channel in order to improve water management in PEMFC. Slanted channels with an angle of 20^o in a flow plate were employed to collect the liquid water. To study the influence of the pore structure and surface wettability on liquid water transport and interfacial dynamics in the PEMFC catalyst layer and GDL, a mesoscopic modeling formalism coupled with realistic microstructural delineation was developed by Mukherjee (2009). Zhu (2011) investigated the effects of the location of droplet entering the channel and the wettability of the sidewall on the dynamic behavior of liquid water in gas channel of fuel cell. Hussaini (2009) investigated the water transport processes in an operating PEMFC and observed four forms of transport such as single-phase flow, droplet flow, film flow and slug flow in the flow channel of PEMFC. Recently, three-dimensional numerical simulations were carried out to investigate the water transport characteristics in the cathode of proton exchange membrane fuel cell with the deformation of gas diffusion layer by Bao (2014).

Using the VOF method, Cai (2006) studied the water droplet and water film movement inside a straight micro-channel of PEMFC to account for the effect of the surface properties on droplet behavior. Dai (2009) reviewed experimental and numerical works on water transport and balance in the membrane electrode assembly of PEMFC and suggested that more interest should be focused to the fundamental understanding and systematic data of water transport in each component of the PEMFC under different operating conditions.

However, most of the previous studies on water droplet removal from a gas channel are limited to a single droplet generated in straight channels, same size and same inlet flow conditions etc. The aim of the present contribution is to improve the fundamental understanding of the effects of surface wettability properties, droplet position, size, droplet's numbers and inlet flow conditions on the water droplet transport in serpentine gas flow channels of PEMFC. Accordingly, in the present study, the water droplet transport in a flow channel with a range of surface wettability properties (contact angle ranges from 140^0 to 160^0 in steps of 10^0), different inlet air velocities and droplet positions have been analyzed by using the VOF method available in the commercial CFD (Computational Fluid Dynamics) software ANSYS Fluent (2010).

2. PROBLEM DESCRIPTION AND NUMERICAL IMPLEMENTATION

A serpentine flow channel of PEM fuel cell having square cross section of 1mm × 1mm and wing length of 8 mm of total 3 wings is chosen as the computational domain (Fig 1). The connecting

length between two wings is 1mm. It is assumed that the liquid water produced in the reaction zone of the cathode side reaches to the flow channels in the form of droplets.

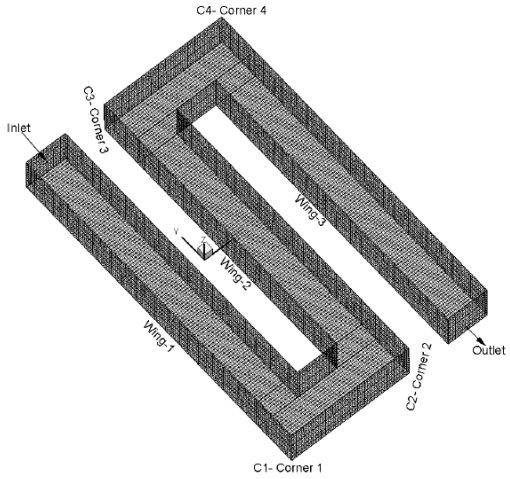

Fig. 1. Schematic diagram of the serpentine gas flow channel.

In the present numerical study, droplet is kept at the center or off-center of the bottom wall (along -z axis) of flow channel and at the center of the top wall (along +z axis). For the sake of simplicity, the following assumptions are made in the present study:

(a) Only single droplet is considered. Droplet is introduced at time, $t > 0$, (b) the motion of gas (air) and water is considered to be an incompressible Newtonian flow, (c) two phases are separated by the interface having a constant surface tension coefficient, (d) there is no phase change for both air and water, (e) surface wettability properties are considered at static condition and (f) the density of air and water are considered at room temperature.

2.1 Governing Equations

The following continuity and momentum equations are solved to study the water droplet transport in single flow channel:

Continuity equation:

$$\frac{\partial \rho}{\partial t} + \nabla.\left(\rho \vec{v}\right) = 0 \tag{1}$$

Momentum equation:

$$\frac{\partial}{\partial t}\left(\rho \vec{v}\right) + \nabla.\left(\rho \vec{v}\vec{v}\right) = -\nabla p + \nabla.\left[\mu\left(\nabla \vec{v} + \nabla \vec{v}^{T}\right)\right] + \rho \vec{g} \tag{2}$$

where $\vec{v}$ is the velocity vector, ρ is the density of the fluid**,** p is the pressure and $\rho \vec{g}$ is the gravity force. The above two equations govern the motion of both air and liquid water in the flow channel. The liquid droplet may deform while moving in the channel and its instantaneous surface is determined by the Volume-of-Fluid (VOF) method. The VOF method and details of its numerical implementation are described in Mondal (2011).

2.2 Initial and Boundary Conditions

Initially $(t = 0)$ all velocities and gauge pressure in the channel are set as zero. At time $t > 0$, a no slip boundary condition is applied to all the channel walls. The air flow at the inlet is considered as fully developed with a parabolic velocity profile having the maximum velocity at the center of the inlet. Channel surface wettability is adjusted by setting different contact angles at the wall. The gravity force is considered along the negative z-direction. The pressure at the channel exit is maintained zero, thus the pressure at the channel inlet will increase when the droplet is introduced into the channel in presence of air flow.

2.3 Numerical Procedure

The unsteady governing equations are solved using a pressure-based solver (ANSYS Fluent 2010) and explicit scheme-based VOF method was selected for the multiphase simulation. Air is considered as the primary phase and liquid water as the secondary phase. In all the simulations, the wall adhesion is considered and the surface tension coefficient (σ) between the air and water is taken a constant value as 0.0734 N/m.

The pressure-implicit with splitting of operators (PISO) scheme is used to obtain the pressure-velocity coupling. The pressure discretizations are obtained by using the PRESTO (pressure staggering option) scheme. The second order upwind scheme is used to solve the momentum equation and the volume fraction at the interface is calculated using the geometric reconstruction scheme. This scheme represents the interface between fluids using a most accurate piecewise-linear approach. The interface between two phases is assumed to be linear within each cell. Based on information about the volume fraction and its derivatives, the position of the linear interface relative to the center of each partially filled cell is calculated. The amount of fluid advected through each face is calculated using the computed linear interface. Then it calculates the normal and tangential velocity distributions on the face. The volume fraction in each cell is calculated using the balance of fluxes obtained during the previous time step. The convergence criteria for the solution of continuity and momentum equations are set in the order of 10^{-5}. A time step size of 10^{-5} sec is used in the computation.

2.4 Grid Independence Test and Validation

In simulation study, acceptable mesh selection is an essential task to come up with satisfactory results. To select the proper mesh size, a comprehensive grid independence test is carried out. Accordingly, three different types of grid sizes ($10\times84\times10$, $16\times128\times16$ and $22\times172\times22$) are chosen for each wing having the total hexahedral cells 27300, 106496 and 270556 respectively in the entire computational domain. The pressure drops are compared for various numbers of hexahedral meshes and shown in Fig. 2. For the finer grid size, it takes more time to completely sweep out the

droplet from the channel and for the coarser grid sizes; the inlet pressure fluctuations are relatively large. Considering the computational time limitation, finally $16\times128\times16$ grid sizes (i.e. 106496 hexahedral meshes) are chosen in the present study to simulate the water droplet transport in the flow channels.

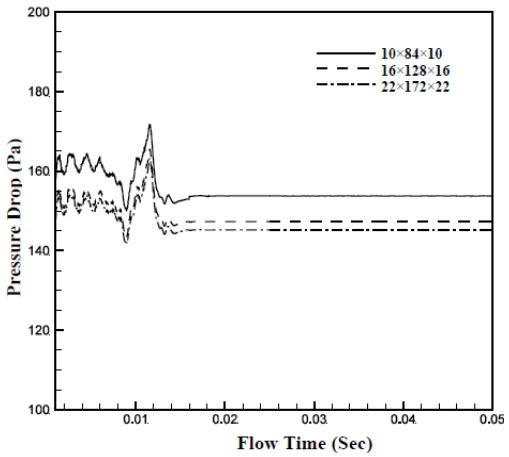

Fig. 2. Grid independence study.

The methodology adopted here for simulating water droplet movement in a serpentine flow channel was tested extensively in (Mondal 2011) for a straight flow channel of PEM fuel cell and excellent results were obtained. Hence, the same has not been repeated here for the purpose of brevity.

3. RESULTS AND DISCUSSION

To investigate the water droplet transport in a serpentine flow channel of a PEMFC, different hydrophobic properties, inlet air velocities, number of droplets, droplet sizes and droplet positions are considered in the present 3-D simulation. Water produced in reaction zone of cathode side is transported into the flow channel through GDL. The droplet is kept at the centre and off-centre of the bottom wall of the flow channel and at the centre of the top wall. The centre (0, 0, 0) of the computational domain is taken at the middle of wing 1 and wing 2. Total 30 cases are simulated to examine the water droplet transport under the following conditions.

Single droplet is introduced at the centre on bottom wall of flow channel $(x=-0.001\text{m}, y=0.0\text{m}, z=-0.0005\text{m})$ for three different inlet velocity boundary conditions (7.5 m/s, 10 m/s and 12.5 m/s) and three different contact angles (140^0, 150^0 and 160^0).

Single droplet is introduced off the centre on the bottom wall of flow channel $(x=-0.0012\text{m}, y=0.0\text{m}, z=-0.0005\text{m})$ for maximum inlet velocity 12.5 m/s and three contact angles (140^0, 150^0 and 160^0).

Single droplet is introduced at centre of the top wall in the flow channel $(x=-0.001\text{m}, y=0.0\text{m}, z=0.0005\text{m})$ for maximum inlet velocity 12.5 m/s and three contact angles (140^0, 150^0 and 160^0).

Single droplet (radius r = 0.0003 m) is introduced at the centre on the bottom wall of flow channel $(x=-0.001\text{m}, y=0.0\text{m}, z=-0.0005\text{m})$ for maximum inlet velocity 12.5 m/s and three contact angles (140^0, 150^0 and 160^0).

Single droplet (radius r = 0.0003 m) is introduced at centre of the top wall in the flow channel $(x=-0.001\text{m}, y=0.0\text{m}, z=0.0005\text{m})$ for maximum inlet velocity 12.5 m/s and three contact angles (140^0, 150^0 and 160^0).

Single spherical droplet (radius r = 0.00025m) is introduced at centre of the top wall in the flow channel $(x=-0.001\text{m}, y=0.0\text{m}, z=0.0005\text{m})$ for maximum inlet velocity 12.5 m/s and three contact angles (140^0, 150^0 and 160^0).

Two droplets are introduced at the centre of the bottom wall in the flow channel (1st wing and 2nd wing) for maximum inlet velocity 12.5 m/s and three contact angles (140^0, 150^0 and 160^0).

Two droplets are introduced at the centre of the top wall in the flow channel (1st wing and 2nd wing) for maximum inlet velocity 12.5 m/s and three contact angles (140^0, 150^0 and 160^0).

Droplet shape depends on the material properties like contact angle, viscosity and surface tension. Inertial force, shear force and pressure differences start to deform droplet when a fluid is forced to pass over a stationary droplet. The surface tension forces and adhesive forces play important roles to keep the droplet spherical and attach to surface. Since the study is conducted at room temperature, a constant value of the surface tension coefficient between air and water $(\sigma = 0.0734\ \text{N/m})$ is used. Standard values of density and viscosity of air and liquid water are also used in all cases.

All the conditions investigated along with the results obtained are enlisted in Tables 1-3. The hemispherical droplet having radius 0.00025m is introduced at the centre of bottom wall $(x=-0.001\text{m}, y=0.0\text{m}, z=-0.0005\text{m})$ for first 9 cases (Case no. 1-9). In next 3 cases (Case no. 10-12), the study has been done for off-centre position of the droplet at bottom wall $(x=-0.0012\text{m}, y=0.0\text{m}, z=-0.0005\text{m})$. In these cases, the hemispherical droplet is placed towards the left wall of first wing. The same size droplet is attached at the centre of top wall $(x=-0.001\text{m}, y=0.0\text{m}, z=0.0005\text{m})$ for the cases (Case no. 13-15). Single droplet with bigger size (radius = 0.0003m) is placed at the centre of on the bottom wall of wing 1 for maximum inlet velocity (12.5 m/sec) for three different contact angles (Case no. 16-18). The same size droplet is also introduced at the centre of the top wall of wing 1 with same inlet velocity and contact angles (Case

Table 1 A list of all the conditions with single droplet size (radius, *r* = 0.00025m) investigated along with results obtained

	U_{max} (m/sec) at center of channel inlet	Reynolds Number (Re)	Contact angle for channel surface (θ^0)	Droplet average speed	Droplet transport time (Sec)
Case. No	Single droplet is introduced at the center on bottom wall of flow channel $(x = -0.001\text{m}, y = 0.0\text{m}, z = -0.0005\text{m})$				
1	12.5	428	140	0.6808	C4-0.0235
2			150	0.6916	0.0347
3			160	0.7777	C3-0.0180
4	10	342	140	0.4285	C2-0.0140
5			150	0.5797	0.0414
6			160	0.6648	0.0361
7	7.5	257	140	0.2857	C2-0.0210
8			150	0.3000	C2-0.0200
9			160	0.4444	C4-0.0360
Single droplet is introduced off the center on the bottom wall of flow channel $(x = -0.0012\text{m}, y = 0.0\text{m}, z = -0.0005\text{m})$					
10	12.5	428	140	0.3809	C1-0.0105
11			150	0.5714	C1-0.0070
12			160	0.8027	0.0299
Single droplet is introduced at center of the top wall in the flow channel $(x = -0.001\text{m}, y = 0.0\text{m}, z = 0.0005\text{m})$					
13	12.5	428	140	0.7430	0.0323
14			150	0.7619	C4-0.0210
15			160	0.7777	C3-0.0180

Table 2 A list of all the conditions with different sizes single droplet investigated along with results obtained

	U_{max} (m/sec) at center of channel inlet	Reynolds Number (Re)	Contact angle for channel surface (θ^0)	Droplet transport time (Sec)
Case. No	Single droplet is introduced at the center on bottom wall of flow channel $(x = -0.001\text{m}, y = 0.0\text{m}, z = -0.0005\text{m})$ and radius of droplet is 0.0003 m.			
16	12.5	514	140	C4-0.0235
17			150	C4-0.0230
18			160	C3-0.0205
Single droplet is introduced at center of the top wall in the flow channel $(x = -0.001\text{m}, y = 0.0\text{m}, z = 0.0005\text{m})$ and radius of droplet is 0.0003 m.				
19	12.5	514	140	C3-0.0185
20			150	C4-0.0245
21			160	C3-0.0213
Single droplet is introduced at center of the top wall in the flow channel $(x = -0.001\text{m}, y = 0.0\text{m}, z = 0.00025\text{m})$ and droplet is spherical in size				
22	12.5	428	140	0.0380
23			150	0.0323
24			160	C3-0.0350

no. 19-21). Another three cases (Case no. 22-24) are run to study the droplet transport phenomena for a spherical droplet with radius = 0.00025m and last six cases (Case no. 25-30) are run to investigate the effects of number of droplets produced at the gas flow channels. In all cases except Cases 4-9, parabolic inlet velocity profiles with maximum velocity (12.5 m/s) at the centre of the inlet are applied. On the basis of droplet diameter and density and viscosity of air, the computed Reynolds

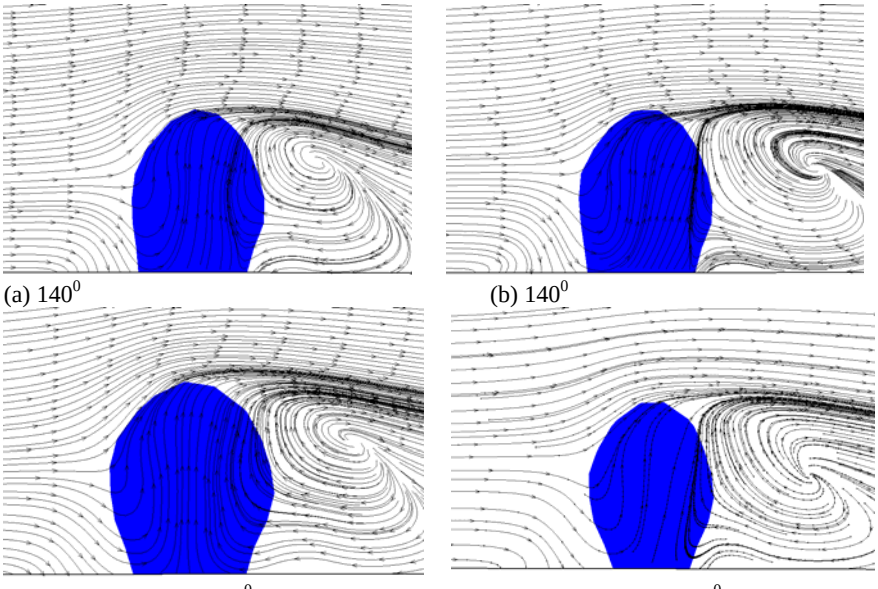

(a) 140^0 (b) 140^0

(c) 160^0 (d) 160^0

Fig. 3. Instantaneous (0.0005sec) contour of streamlines at the y-z plane for three different contact angles (140^0 and 160^0); (a) and (c) for the maximum inlet velocity 7.5m/sec; (b) and (d) for the maximum inlet velocity 12.5m/sec.

Table 3 A list of all the conditions with two droplets (radius, *r* = 0.25mm) investigated along with results obtained

	U_{max} (m/sec)	Re	Contact angle	Droplet removal time from 2nd wing (Sec)	Droplet removal time from 1st wing (Sec)
Case. No	Two droplets are introduced at center of the bottom wall in the flow channel (1st wing and 2nd wing)				
25	12.5	428	140	0.0347	0.0347
26			150	0.0179	0.0349
27			160	0.0174	C3-0.0190
Two droplets are introduced at center of the top wall in the flow channel (1st wing and 2nd wing)					
28	12.5	428	140	0.0349	0.0349
29			150	0.0177	0.0280
30			160	0.0183	C3-0.0225

numbers are listed for all cases. A wide range of surface wettability properties (140^0, 150^0 and 160^0) are considered to study the effect of hydrophobic property of walls on droplet transport. The average droplet speeds are calculated approximately on the basis of distance covered by the droplet and time taken by the droplet to reach there. Due to less contact area for high value of contact angle, the average speed is more compared to other two contact angles. With high contact angle (160^0) and even at minimum considered inlet velocity (7.5 m/s), the droplet is detached from the bottom wall and reached the top wall. Whereas, with small contact angle (140^0) and maximum considered inlet velocity (12.5 m/s), the droplet is attached always with either bottom wall or side walls of the flow channels. Due to smaller contact angle (140^0), the contact area of droplet and wall is more compared to other two contact angles; hence more surface tension force is applied for this case. However, with maximum inlet velocity (12.5 m/s), sufficient lift force is not developed to detach the droplet from bottom wall of the channel with contact angles of 140^0. The highlighted values in the last column of Table 1-3 indicate the time required for the droplet to escape from the serpentine flow channel and other values indicate the time required to reach the droplet at the corner position mentioned. The minimum droplet removal time is found for Case no. 29 and maximum removal time is observed for Case no. 5.

Instantaneous streamline contours and droplet shapes at the mid y-z plane of wing 1 for two different contact angles (140^0 and 160^0) with the minimum velocity 7.5 m/sec at the inlet centre (Case 7 and 9 in Table 1, respectively) and maximum12.5 m/sec at the inlet centre (Case 1 and 3 in Table 1, respectively) are shown in Fig 3. The droplet is introduced at the bottom wall centre of the middle of the wing 1 $(x = -0.001\text{m}, y = 0.0\text{m}, z = -0.0005\text{m})$ for above mentioned cases. Due to hydrophobic surface properties, the shape of the droplet changes

gradually and takes appropriate shape according to the contact angle. The results are shown for a particular time instant, 0.0005 sec. At the beginning of simulation for both cases, the droplet moves very slow because of its unstable shape at that moment. As surface contact area increases, adhesive force increases and pressure force and drag force decreases which results slow motion of the droplet. As surface contact with the bottom wall decreases, the adverse pressure gradient increases and the flow recirculation (vortex) appears behind the droplet from the very beginning of the computations.

Due to brevity of the manuscript, a specified contact angle of 150^0 is considered for studying the effects of inlet air velocity on inlet as shown in Fig. 4. Initially, the inlet pressure fluctuates and magnitude of fluctuation highly depends on the inlet air velocity conditions. The inlet pressure is larger for higher inlet air velocity. The pressure remains almost constant either in case of when droplet goes out of channel or stacks at the corner of the channel.

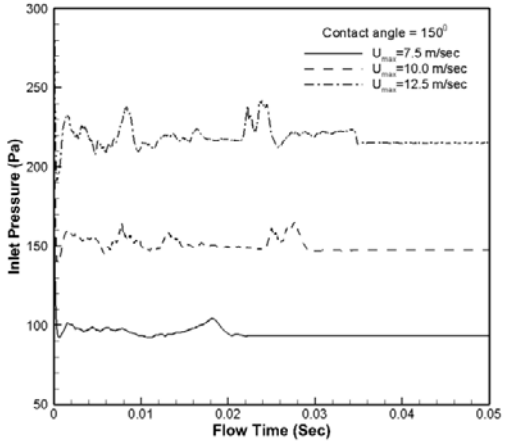

Fig. 4. Effects of inlet velocity on pressure drop at the serpentine flow channel when a liquid water droplet is introduced at the centre of bottom wall.

Figure 5 shows the inlet pressure fluctuation for different contact angles with a specified inlet air velocity (10 m/sec) boundary condition. In this case, initially the inlet pressure fluctuates and reaches same minimum pressure generated at the inlet of the channel due to the air flow only for all contact angles. At the very beginning, the pressure at the inlet is very high as a result of the sudden presence of droplet within the channel.

Figures 6-8 show the 3-D views of droplet transport positions for different hydrophobic surface properties with three different maximum inlet velocities at different time instants. The droplet is introduced at bottom wall centre $(x=-0.001\text{m}, y=0.0\text{m}, z=-0.0005\text{m})$ of wing 1 of the gas flow channels. The droplet is stuck at corner 2 (C2) when the maximum inlet velocity is 7.5 m/sec and the contact angle (CA) is 140^0. It takes time 0.0210 sec to reach at C2.

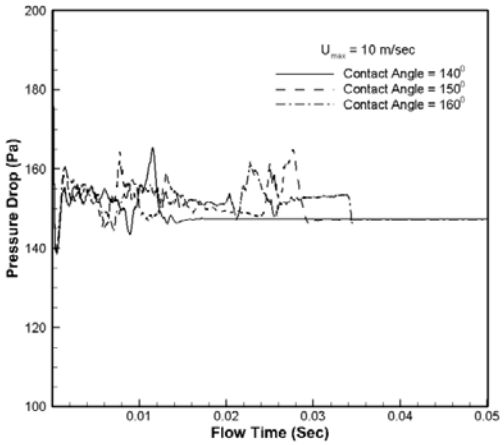

Fig. 5. Effects of contact angle on pressure drop at the serpentine flow channel when a liquid water droplet is introduced at the centre of bottom wall.

The similar phenomenon is also observed for the more hydrophobic surface properties (Contact angle 150^0) with same inlet velocity profile. Due to high hydrophobic properties, the contact area between droplet and surface of the channel is less and the droplet takes less time to reach at C2 (Fig. 6b and Case no. 14). For the case of super hydrophobic property (CA 160^0), the droplet is moved forward and finally trapped at C4 (Fig 6c).

Figure 7 shows the droplet transport phenomena for three different contact angles with maximum velocity 10m/sec at the centre of inlet of the flow channel. The droplet takes the position at corner 2 (C2) for CA 140^0 (Fig 7a) and time taken by the droplet to reach at C2 is 0.014sec. Due to low drag force at the corner and the presence of recirculation, the droplet is completely stuck there throughout the entire simulation i.e. 0.05sec.

The droplet escapes from the serpentine flow channel for CA of 150^0 (Fig 7b) and 160^0(Fig 7c). Due to less contact area of liquid water and surface of wall, the lift force dominates over the surface tension force and the droplet detaches from the bottom wall and then touches the top wall of the channel in both cases. It collides with the side wall of wing 2 and moves forward. Finally the droplet escapes from the serpentine flow channel at time t = 0.0414sec for CA of 150^0 whereas it takes comparatively less time for CA of 160^0.

The different phenomena in case of droplet transport within the serpentine gas flow channel with maximum inlet velocity 12.5 m/sec are shown in Fig 8. The droplet is completely removed from the gas flow channel when the CA is 150^0 but it is stuck at the corners with less (140^0) or more (160^0) hydrophobic properties of the channel surfaces. Due to high recirculation and less drag force at the corners, the droplet is trapped at the corners (C4 and C2) at time 0.0235 sec for CA 140^0 and 0.0180 sec for CA 160^0, respectively. The droplet is completely escaped from the flow channel at 0.0347 sec for CA 150^0.

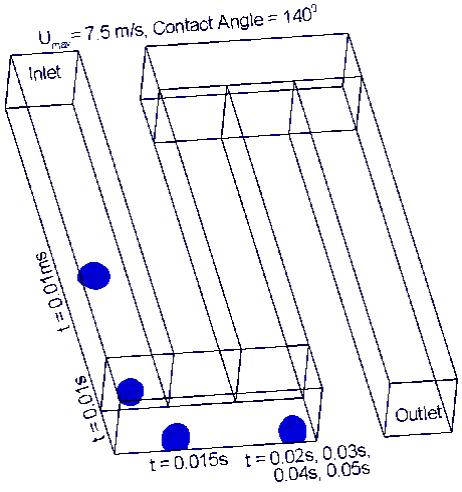

(a)

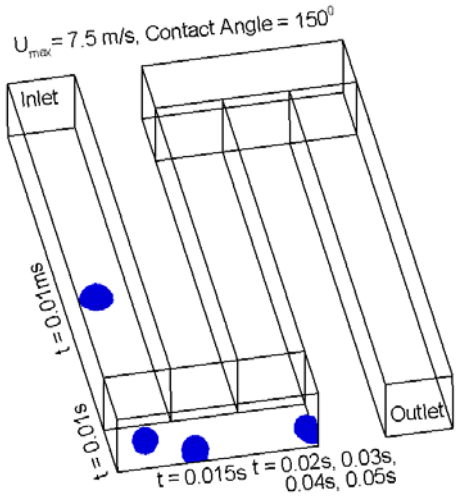

(b)

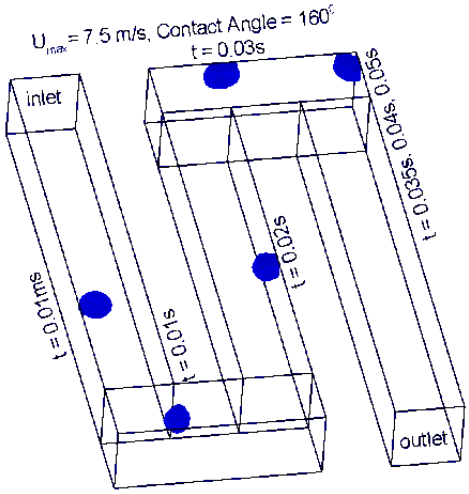

(c)

Fig. 6. Droplet transport (center of bottom wall) at different instants on hydrophobic surfaces for the maximum inlet velocity 7.5m/sec for various CA (a) 140^0, (b) 150^0 and (c) 160^0.

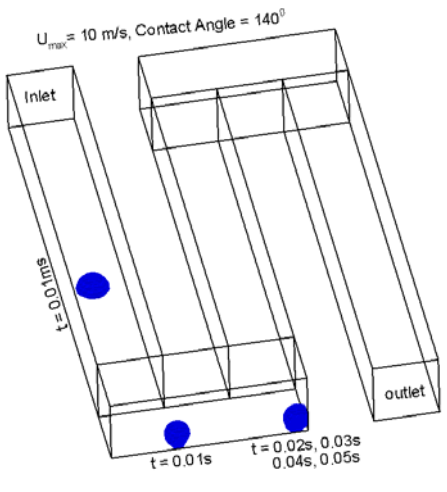

(a)

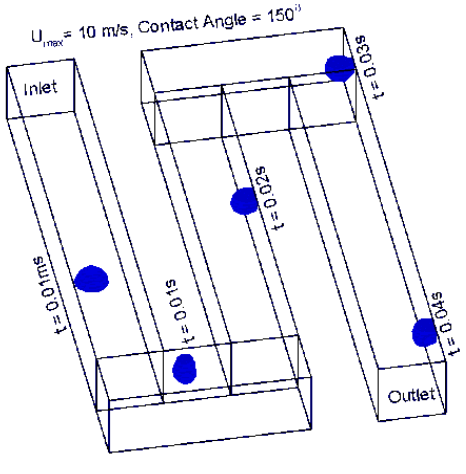

(b)

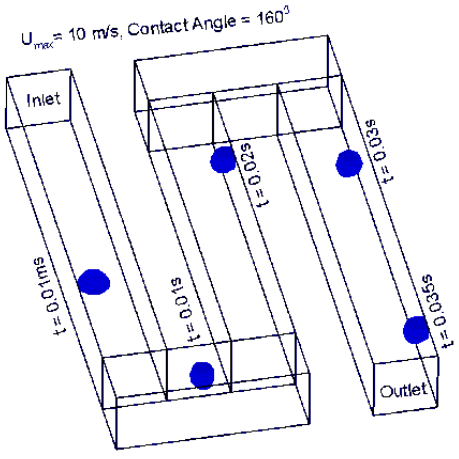

(c)

Fig. 7. Droplet transport (center of bottom wall) at different instants on hydrophobic surfaces for the maximum inlet velocity 10m/sec for various CA (a) 140^0, (b) 150^0 and (c) 160^0.

In Fig 9, the 3-D views of droplet positions are shown for different hydrophobic surface properties with the maximum air velocity 12.5 m/sec at the centre of the channel inlet at different time instants. The droplet is introduced at off-centre position of middle of the bottom wall of wing

$1\left(x=-0.0012\text{m}, y=0.0\text{m}, z=-0.0005\text{m}\right)$. Three contact angles ($140^0$, 150^0 and 160^0) are considered to study the effect of droplet position on the droplet transport. In Fig 9a, the droplet positions are shown for the contact angle of 140^0. Due to off-centre position, it moves towards the right side wall of wing 1 due to unequal pressure force and sticks with the side wall very quickly. Finally, it reaches at the corner position C1 at time 0.0105 sec. The same phenomenon is also observed for higher contact angles of 150^0 (Fig 9b). With CA of 150^o, it detaches from the bottom wall and floats in the air. Finally the droplet reaches to the side wall of wing 1 due to unequal pressure force and sticks at C1. For the super hydrophobic surface property of CA of 160^o (Fig 9c), it is lifted up quickly and moves forward as a floating body and then collides at the front wall near C1. Then it touches the top wall and changes the direction gradually from the right side wall to the left side wall. Then it collides again with the right wall of the wing 2. For this case, it moves forward while touches the top wall as well as one side wall also. Finally, the droplet is completely swept out from the flow channel at time t = 0.0299 sec.

The droplet positions at different time instants are shown in Fig 10. The same size droplet is introduced at centre of the top surface $\left(x=-0.001\text{m}, y=0.0\text{m}, z=0.0005\text{m}\right)$ of wing 1. The parabolic velocity profile with maximum velocity 12.5 m/s is applied at the inlet of the serpentine channel. The surface wettability properties are maintained by imposing proper values of the contact angles. The droplet positions at five time instants are shown for the CA of 140^0

(Fig 10a). At time t = 0.01ms, the droplet holds almost at the starting point. Due to high contact area that results in higher surface tension force, it does not detach from the top surface throughout the entire simulation. At time t = 0.02 sec, the droplet looks like a bigger size because of deformation of the droplet with high thrust force. Finally, it is escaped from the channel at time t = 0.0323 sec. However, the droplet is trapped for other two cases (Case no 14 and Case no 15 in Table 1). Due to the gravitational force, the droplet is detached from the top surface and moved forward as a floating body throughout the entire wing 1 for the CA of 150^0 (Fig 10b). Droplet touches the wall again and moves forward. Finally, at time t = 0.021 it is stuck at the corner 4 (C4) and remained at the same corner until the end of simulation.

It is to be noted that due to high impact collision of water droplet at the end of wing 2, a small part of the droplet is separated and stuck at C3. In Fig 10c, the droplet comes to the bottom wall very quickly. The droplet detaches again from the bottom wall and moves forward. At time t = 0.0125, the droplet touches the left wall of wing 2 and moves forward. Then it is finally trapped at C3 because of the fact that the surface tension force dominates over the drag force at the corners.

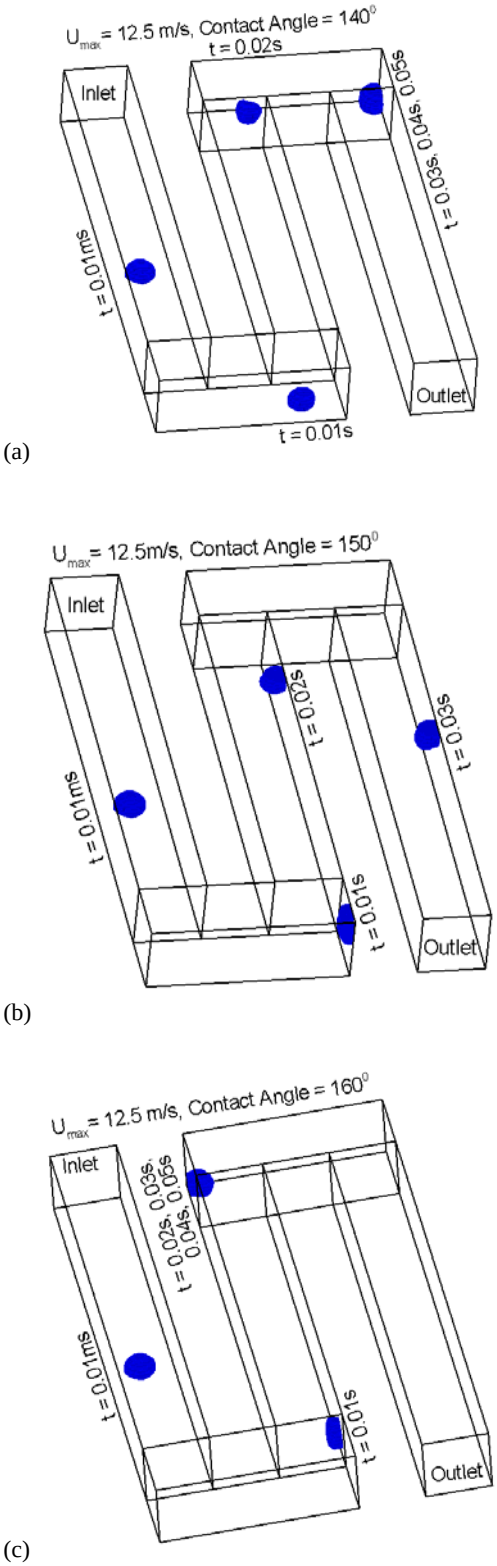

Fig. 8. Droplet transport (center of bottom wall) at different instants on hydrophobic surfaces for the maximum inlet velocity 12.5m/sec for various CA (a) 140^0, (b) 150^0 and (c) 160^0.

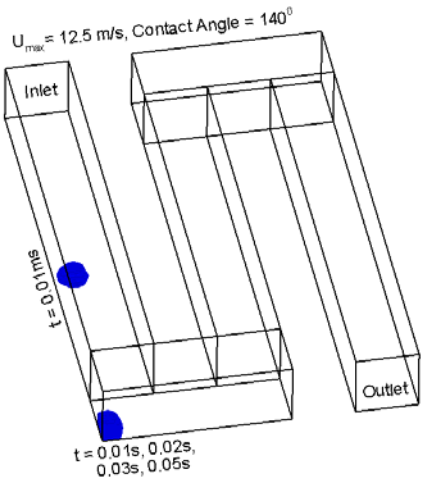

(a)

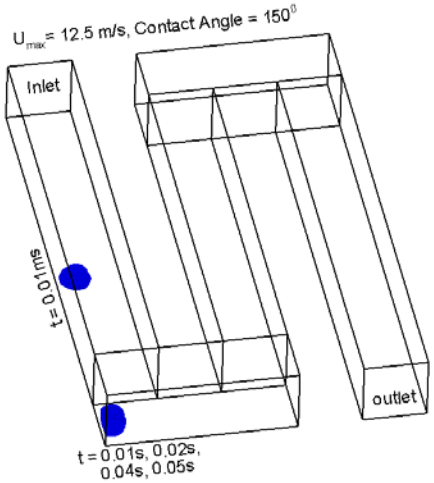

(b)

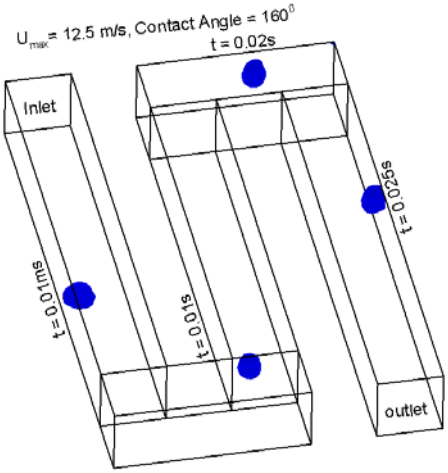

(c)

Fig. 9. Droplet transport (off-center position) at different instants on hydrophobic surfaces for the maximum inlet velocity 12.5m/sec for various CA (a) 140^0, (b) 150^0 and (c) 160^0.

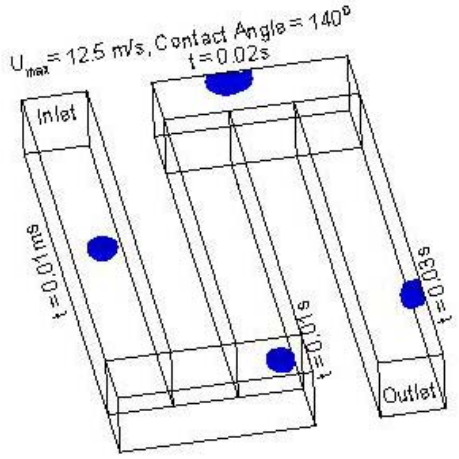

(a)

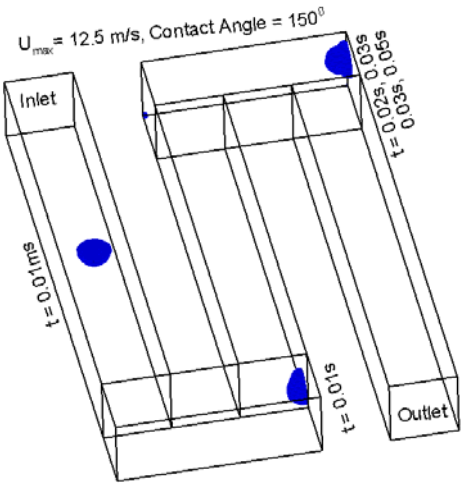

(b)

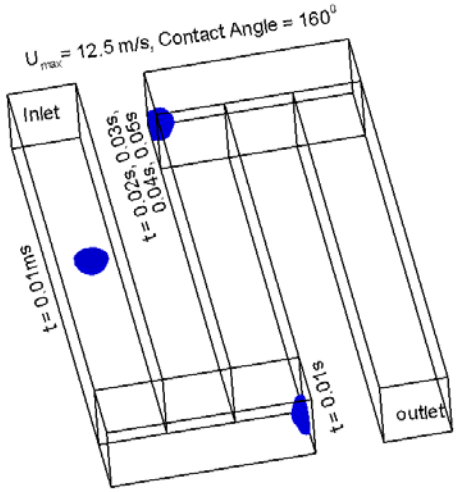

(c)

Fig. 10. Droplet transport (top surface) at different instants on hydrophobic surfaces for the maximum inlet velocity 12.5m/sec forvarious CA (a) 140^0, (b) 150^0 and (c) 160^0.

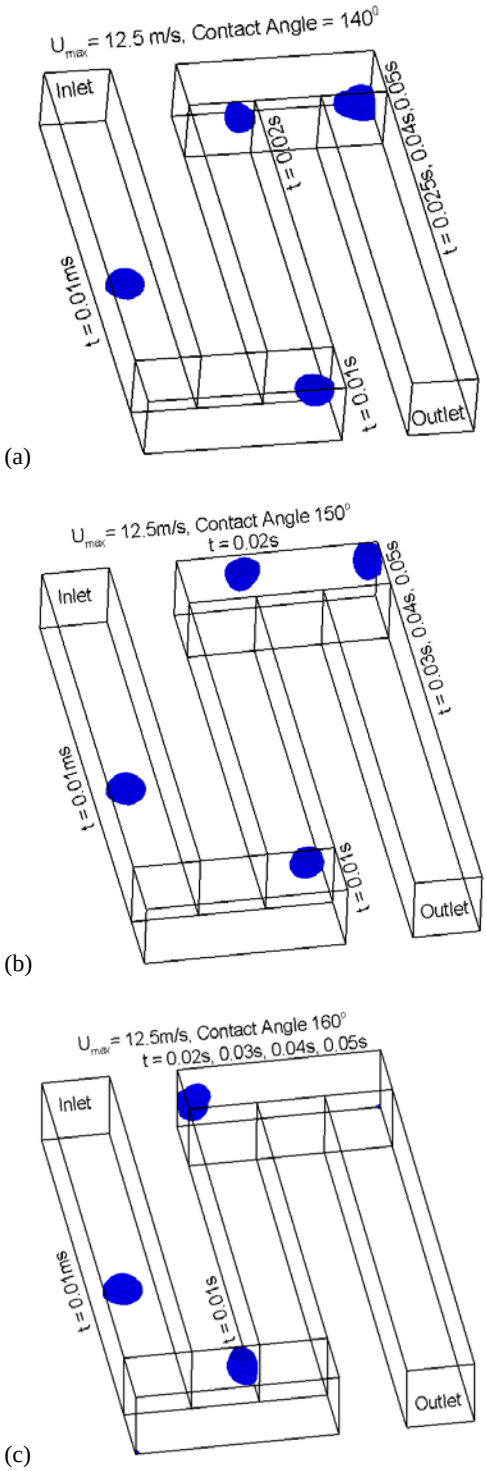

Fig. 11. Droplet (r = 0.0003m) transport (bottom surface) at different instants on hydrophobic surfaces for the maximum inlet velocity 12.5m/sec for various CA (a) 140^0, (b) 150^0 and (c) 160^0.

The droplet transport phenomena are also compared with different sizes of droplet used in the simulation study. Figure 11 and 12 show the effects of droplet size (Case no. 16-21 in Table 2) on the droplet transport within the serpentine gas flow channel of the PEMFC. In Fig 11, the droplet with radius, *r* = 0.0003m is introduced at the centre of the bottom surface of wing 1 in the computational domain. Comparing Fig 8 (Case no 1-3) and Fig 11 (Case no 16-18) or Case no 1-3 and Case no 16-18, it is observed that not even a single droplet is completely escaped from the gas flow channel in case of bigger size droplet generated in the channel.

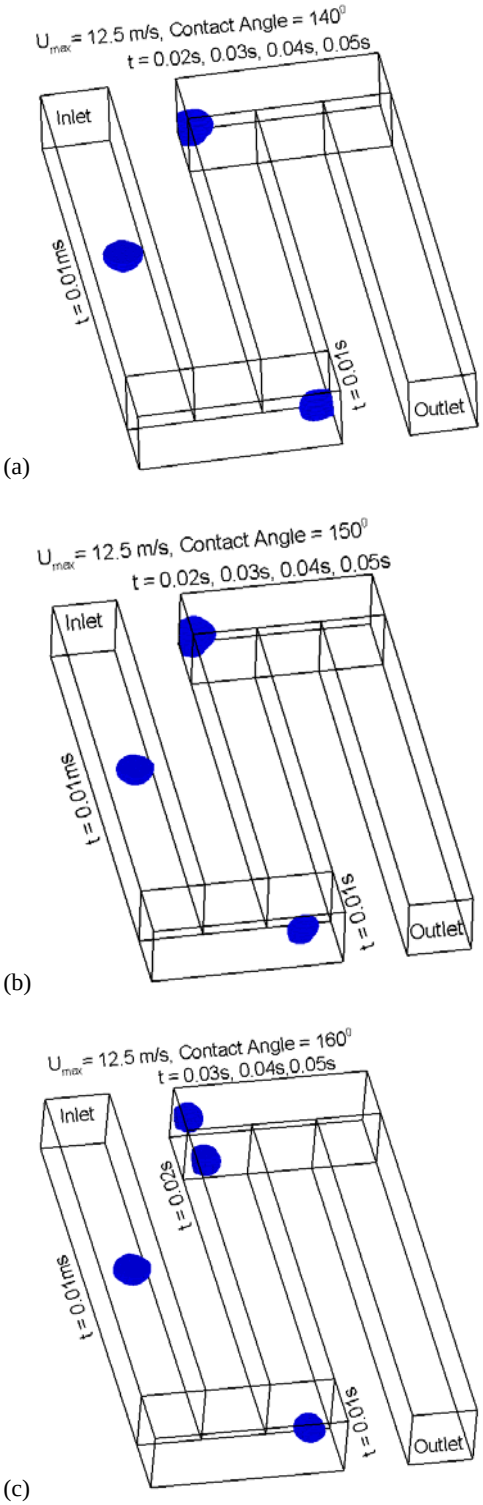

Fig. 12. Droplet (r = 0.0003m) transport (top surface) at different instants on hydrophobic surfaces for the maximum inlet velocity 12.5m/sec for various CA (a) 140^0, (b) 150^0 and (c) 160^0.

However, if the droplet is introduced in the top surface of the 1st wing of flow channel, the smaller size droplet is completely escaped for CA 140^0. Bigger size droplet introduced at top surface of the 1st wing of flow channel is trapped at one of the corners of the serpentine channel with hydrophobic surface properties and maximum inlet velocity 12.5 m/sec (Fig 12 and Case no.19-21).

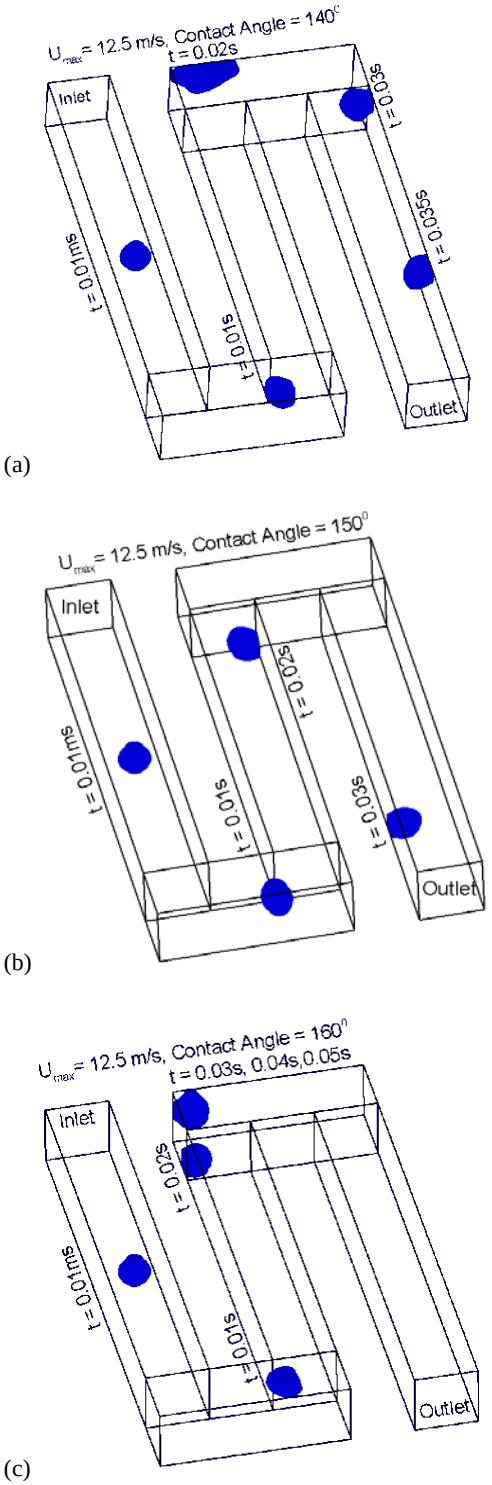

Fig. 13. Spherical size droplet transport at different instants on hydrophobic surfaces for the maximum inlet velocity 12.5m/sec for various CA (a) 140^0, (b) 150^0 and (c) 160^0.

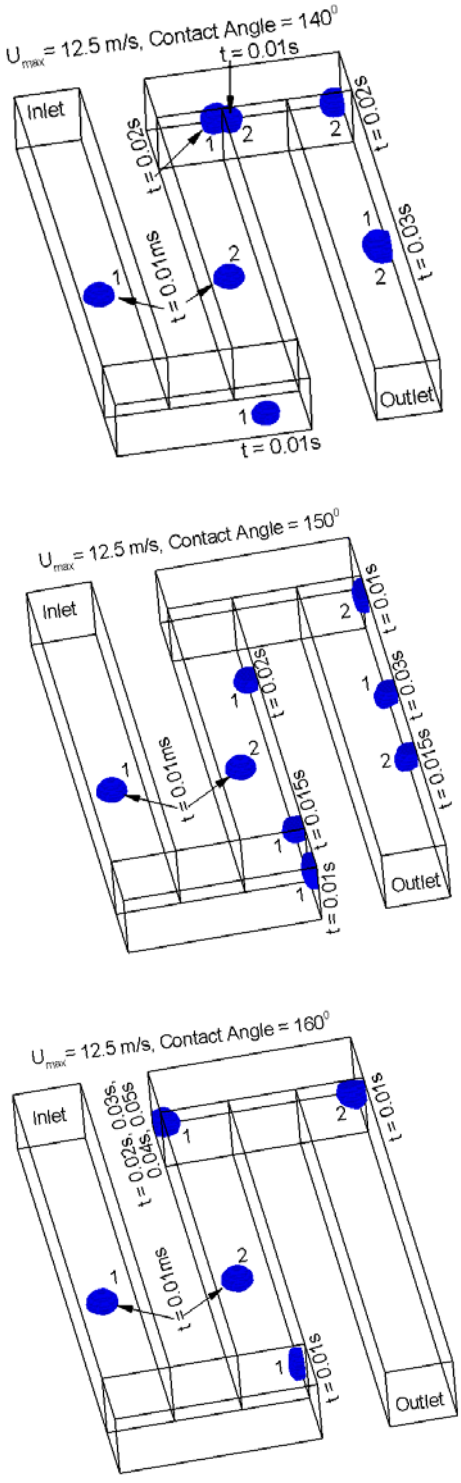

Fig. 14. Two droplets transport (center of bottom wall) at different instants on hydrophobic surfaces for the maximum inlet velocity 12.5m/sec for various CA (a) 140^0, (b) 150^0 and (c) 160^0.

Fig 13 shows the spherical size droplet transport position for three different hydrophobic properties with maximum inlet velocity 12.5 m/sec.

The droplet is introduced at the centre of the top surface of wing 1 in the flow channel (Case no 22-24). For the case of spherical size droplet with CA

140^0 and 150^0, the droplet is completely escaped from the gas flow channel; however the droplet is trapped at C3 for the case of super hydrophobic surface property (CA 160^0). Comparing the hemispherical size droplets (Case No 13-15) and spherical size droplets (Case no 22-24), it is noticed that the droplet is completely escaped in case of CA 140^0 (Case no 13 and 22).

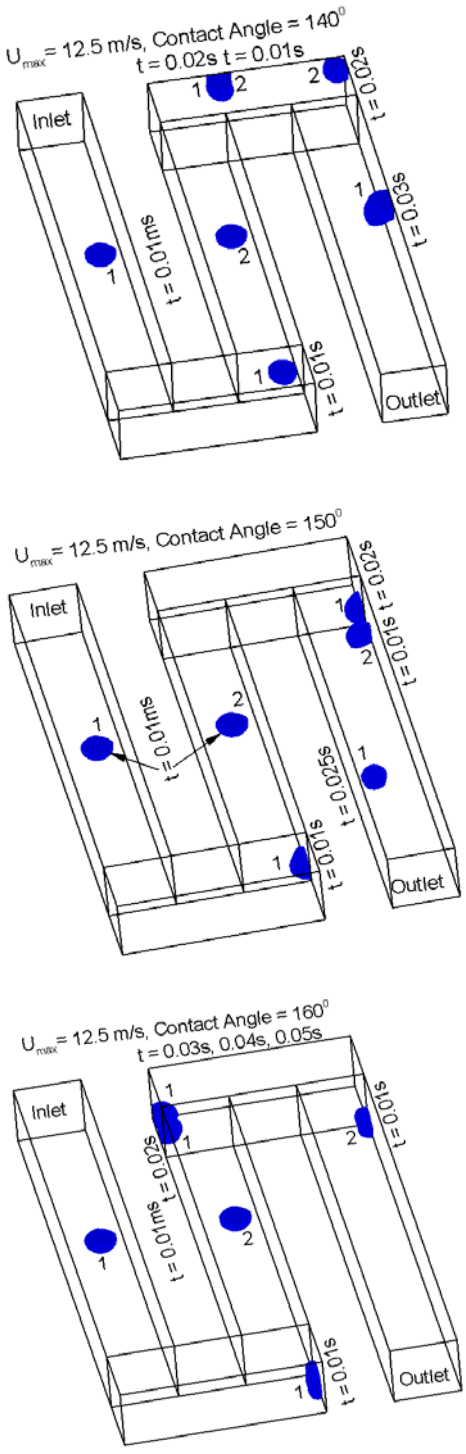

Fig. 15. Two droplets transport (center of top wall) at different instants on hydrophobic surfaces for the maximum inlet velocity 12.5m/sec for various CA (a) 140^0, (b) 150^0 and (c) 160^0.

Droplet removal time is more for the spherical size droplet compared to hemispherical droplet as shown in Table 1 (Case no 13) and 2 (Case no 22).

The droplet transport phenomena with two droplets introduced in the same time at two different wings of the channel are shown in Figs 14 and 15. Two droplets introduced at centers of the bottom of the channel are shown in Fig 14 (Case no 25-27).

The maximum inlet velocity considered is 12.5 m/sec. Due to high thrust at wing 1, the droplet introduced at wing 1 moves very fast and two droplets forms almost a single droplet at time t = 0.01sec, then two droplets completely escape from the channel at t = 0.0347s (Fig.14a and Case no. 25). In case of more hydrophobic properties of the surface (CA 150^0), the droplets completely escape from the channel taking time t = 0.0349 and 0.0179 sec for droplet introduced at wing 1 and wing 2, respectively (Fig 14b and Case no 26). Figure 14c shows the droplet movements for CA 160^0. For this case, the droplet introduced at wing 2 completely escapes from the flow channel at time t = 0.0174 sec, however the droplet introduced at wing 1 is trapped at C3 at time t = 0.0190 sec.

Similar phenomena can also be observed when the droplets are introduced at the centers of the top surfaces of the channel instead of bottom of the surfaces. Two droplets completely escape from the channel for the cases with maximum inlet velocity 12.5 m/sec and CA of 140^0 at the same time t = 0.0349 sec (Fig 15a and Case no 28). With CA of 150^0, two droplets completely escape from the channel at time t = 0.0280 and 0.0177 sec for droplets introduced at wing 1 and wing 2, respectively (Fig 15b and Case no 29). The droplet introduced at wing 1 is trapped at C3 at time t = 0.0225 sec and second droplet completely escapes at time t = 0.0183 sec when the CA is 160^0 (Fig 15c and Case no 30).

4. CONCLUSION

To understand the fundamental phenomena of the water droplet transport in a serpentine gas flow channel of PEMFC, a comprehensive three dimensional numerical simulation is carried out by using the commercial CFD package FLUENT. Total 30 cases of different combinations of air flow conditions, channel surface wettability, droplet positions, droplet sizes and droplet numbers are studied. The droplet movement is significantly affected by the above parameters. The droplet is not removed for any kind of surface properties with parabolic velocity profile having maximum velocity 7.5 m/sec at the centre of inlet. Due to low drag force, the droplet is trapped one of the corners of the channel. In case of parabolic velocity profile with maximum inlet velocity 10 m/s at the centre of inlet, the effective surface wettability property is 160^0. With maximum inlet velocity 10 m/sec, it takes the minimum time to completely remove the droplet from the channel when the CA is 160^0. The average droplet speed is higher for

higher values of CA as expected. However, the high (CA 160^0) surface wettability property is not suitable for water management in PEMFC channel. In case of centre position of droplet on the bottom wall with maximum inlet velocity (12.5 m/s), the preferable CA is 150^0. The droplet is completely removed from the flow channel only with CA of 160^0 and maximum inlet velocity 12.5 m/s for the droplet off centre position on the bottom wall. The opposite trend is observed in case of droplet attachment at top wall of wing 1 in the flow channel. In this case, the preferable surface wettability property is 140^0. The droplet with bigger size is not escaped from the channel neither for droplet introduced at bottom / top surfaces or contact angles with maximum inlet velocity 12.5 m/sec. The spherical size droplet is completely escaped from the channel with comparatively lower hydrophobic surface properties. For the case of two droplets introduced in different wings at the same time, the lower hydrophobic properties are preferable for better droplet removal from the channel. Therefore, hydrophobic surface property depending upon the inlet velocity and droplet position is required to design the flow channels of the bipolar plate.

ACKNOWLEDGEMENT

This work was financially supported by Department of Science & Technology (Project No. GAP-182712) and Indo-US Research Fellowship Program-2013.

REFERENCES

ANSYS Workbench User's Guide (2010). Release 13.0, ANSYS Inc., Canonsburg, PA.

Bao, N., B. Zhou, K. Jiao, Y. Yin and Q. Du (2014). Effect of gas diffusion layer deformation on liquid water transport in proton exchange membrane fuel cell. *Engineering Applications of Computational Fluid Mechanics* 8, 26-43.

Bunmark, N., S. Limtrakul, M. W. Fowler, T. Vatanatham and J. Gostick (2010). Assisted water management in a PEMFC with a modified flow field and its effect on performance. *International Journal of Hydrogen Energy* 35, 6887-6896.

Cai, Y. H., J. Hu, H. P. Ma, B. L. Yi and H. M. Zhang (2006). Effects of hydrophilic /hydrophobic properties on the water behavior in the micro-channels of a proton exchange membrane fuel cell. *Journal of Power Sources* 161, 843-848.

Cho, S. C., Y. Wang and K. S. Chen (2012). Droplet dynamics in a polymer electrolyte fuel cell gas flow channel: Forces, deformation, and detachment. I: Theoretical and numerical analyses. *Journal of Power Sources* 206, 119-128.

Dai, W., H. Wang, X.-Z. Yuan, J. J. Martin, D. Yang, J. Qiao and J. Ma (2009). A review on water balance in the membrane electrode assembly of proton exchange membrane fuel cells. *International Journal of Hydrogen Energy* 34, 9461-9478.

Esposito, A., A. D. Montello, Y. G. Guezennec and C. Pianese (2010). Experimental investigation of water droplet–air flow interaction in a non-reacting PEM fuel cell channel. *Journal of Power Sources* 195, 2691-2699.

Golpaygan, A., A. Sarchami and N. Ashgriz (2011). Three-dimensional multiphase flow model to study channel flow dynamics of PEM fuel cells. *International Journal of Energy Research* 35, 1188–1199.

Hussaini, I. S. and C. Y. Wang (2009). Visualization and quantification of cathode channel flooding in PEM fuel cells. *Journal of Power Sources* 187, 444-451.

Issa R. I. (1986). Solution of the implicitly discretized fluid flow equations by operator splitting. *Journal of Computational Physics* 62, 40-65.

Jiao, K., B. Zhou and P. Quan (2006). Liquid water transport in parallel serpentine channels with manifolds on cathode side of a PEM fuel cell stack. *Journal of Power Sources* 154, 124-137.

Jiao, K., B. Zhou and P. Quan (2006). Liquid water transport in straight micro-parallel-channels with manifolds for PEM fuel cell cathode. *Journal of Power Sources* 157, 226-243.

Jiao, K., J. Park and X. Li (2010). Experimental investigations on liquid water removal from the gas diffusion layer by reactant flow in a PEM fuel cell. *Applied Energy* 87, 2770-2777.

Kumbur, E. C., K. V. Shar and M. M. Mench (2006). Liquid droplet behavior and instability in a polymer electrolyte fuel cell flow channel. *Journal of Power Sources* 161, 333-345.

Lu, Z., M. M. Daino, C. Rath and S. G. Kandlikar (2010). Water management studies in PEM fuel cells, Part III: Dynamic breakthrough and intermittent drainage characteristics from GDLs with and without MPLs. *International Journal of Hydrogen Energy* 35, 4222-4233.

Martemianov, S., M. Gueguen, J. C. Grandidier and D. Bograchev (2009). Mechanical effects in PEM fuel cell: application to modeling of assembly procedure. *Journal of Applied Fluid Mechanics* 2, 49-54.

Mondal, B., K. Jiao and X. Li, (2011). Three dimensional simulation of water droplet movement in PEM fuel cell flow channels. *International Journal of Energy Research* 35, 1200-1212.

Mukherjee, P. P., C. Y. Wang and Q. Kang (2009). Mesoscopic modeling of two-phase behavior and flooding phenomena in polymer electrolyte fuel cells. *Eletrochemica Acta* 54, 6861-6875.

Nguyen, T. V. and M. W. Knobbe (2003). A liquid water management strategy for PEM fuel cell stacks. *Journal of Power Sources* 114, 70-79.

Park, J. and X. Li (2007). An experimental and numerical investigation on the cross flow through gas diffusion layer in a PEM fuel cell with a serpentine flow channel. *Journal of Power Sources* 163, 853-863.

Peyret R., Handbook of Computational Fluid Mechanics (1996). Academic Press Limited, USA.

Qi, Z. and A. Kaufman (2002). Improvement of water management by a microporous sublayer for PEM fuel cells. *Journal of Power Sources* 109, 38-46.

Qin, Y., Q. Du, Y. Yin, K. Jiao and X. Li (2013). Numerical investigation of water dynamics in a novel proton exchange membrane fuel cell flow channel. *Journal of Power Sources* 222, 150-160.

Theodorakakos, A., T. Ous, M. Gavaises, J. M. Nouri, N. Nikolopoulos and H. Yanagihara (2006). Dynamics of water droplets detached from porous surfaces of relevance of PEM fuel cells. *Journal of Colloid and Interface Science* 300, 673-687.

Wang Y., S. A. Shakhshir, X. Li and P. Chen (2012). Superhydrophobic flow channel surface and its impact on PEM fuel cell performance. *International Journal of Low Carbon Technology* 0, 1-12.

Yi, J. S., J. D. Yang and C. King (2004). Water management along the flow channels of PEM fuel cells. *American Institute of Chemical Engineers (AIChE) Journal* 50, 2594-2603.

Zhu, X., P. C. Sui, N. Djilali and Q. Liao (2011). Dynamics of emerging water droplet subjected to sidewall with different wettabilities in a fuel cell cathode channel. *Fuel Cells* 1, 404–412.